Cerebral Cortex, July 2018;28: 2622–2635

doi: 10.1093/cercor/bhy089
Advance Access Publication Date: 9 May 2018
Original Article

ORIGINAL ARTICLE

RIPK3/MLKL-Mediated Neuronal Necroptosis Modulates the M1/M2 Polarization of Microglia/Macrophages in the Ischemic Cortex

Jiping Yang[1,2], Youyi Zhao[1,3], Li Zhang[1,2], Hong Fan[1], Chuchu Qi[1], Kun Zhang[1], Xinyu Liu[1], Lin Fei[4], Siwei Chen[1], Mengmeng Wang[1], Fang Kuang[1], Yazhou Wang[1] and Shengxi Wu[1]

[1]Department of Neurobiology and Institute of Neurosciences, School of Basic Medicine, Fourth Military Medical University, 169 Chang Le Xi Road, Xi'an, Shaanxi 710032, China, [2]Department of Anatomy, Shaanxi Key Laboratory of Brain Disorders and Institute of Basic Medical Sciences, Xi'an Medical University, 1 Xin Wang Road, Xi'an, Shaanxi 710021, China, [3]School of Basic Medicine, Chengdu Medical College, Chengdu 610500, China and [4]Department of Psychiatry, The First Affiliated Hospital of Xi'an Jiaotong University, 277 Yan Ta Western Road, Xi'an, Shaanxi 710061, China

Address correspondence to Dr Shengxi Wu, Department of Neurobiology, Institute of Neurosciences, School of Basic Medicine, Fourth Military Medical University, 169 Chang Le Xi Road, Xi'an, Shaanxi 710032, China. Email: shengxi@fmmu.edu.cn; Dr Yazhou Wang, Department of Neurobiology, Institute of Neurosciences, School of Basic Medicine, Fourth Military Medical University, 169 Chang Le Xi Road, Xi'an, Shaanxi 710032, China. Email: yazhouw@fmmu.edu.cn

Jiping Yang, Youyi Zhao, and Li Zhang contribute equally to the work.

Abstract

Cell death and subsequent inflammation are 2 key pathological changes occurring in cerebral ischemia. Active microglia/macrophages play a double-edged role depending on the balance of their M1/M2 phenotypes. Necrosis is the predominant type of cell death following ischemia. However, how necrotic cells modulate the M1/M2 polarization of microglia/macrophages remains poorly investigated. Here, we reported that ischemia induces a rapid RIPK3/MLKL-mediated neuron-dominated necroptosis, a type of programmed necrosis. Ablating RIPK3 or MLKL could switch the activation of microglia/macrophages from M1 to the M2 type in the ischemic cortex. Conditioned medium of oxygen-glucose deprivation (OGD)-treated wild-type (WT) neurons induced M1 polarization, while that of RIPK3$^{-/-}$ neurons favored M2 polarization. OGD treatment induces proinflammatory IL-18 and TNFα in WT but not in RIPK3$^{-/-}$ neurons, which in turn upregulate anti-inflammatory IL-4 and IL-10. Furthermore, the expression of Myd88—a common downstream adaptor of toll-like receptors—is significantly upregulated in the microglia/macrophages of ischemic WT but not of RIPK3$^{-/-}$ or MLKL$^{-/-}$ cortices. Antagonizing the function of Myd88 could phenocopy the effects of RIPK3/MLKL-knockout on the polarization of microglia/macrophages and was neuroprotective. Our data revealed a novel role of

necroptotic neurons in modulating the M1/M2 balance of microglia/macrophages in the ischemic cortex, possibly through Myd88 signaling.

Key words: cerebral ischemia, microglia/macrophage, necroptosis, polarization

Introduction

Cell death and inflammation are the 2 hallmark pathological changes occurring after an ischemic stroke (Vidale et al. 2017). Innate immunity, characterized by the activation of resident microglia and recruitment of bone marrow-derived macrophages, is the first line of postischemic inflammation in the brain (Stoll et al. 1998; An et al. 2014). Microglia and macrophages are activated and recruited by injury signals, such as ATP released from damaged cells (Yenari et al. 2010; Ma et al. 2017). Activated microglia/macrophages usually switch their phenotypes between 2 polarized conditions (Lan et al. 2017; Ma et al. 2017). One is the M1 type, which expresses proinflammatory factors and functions to remove dead cells and clear tissue debris. The other is the M2 type, which expresses anti-inflammatory and growth factors to help with the reparation of damaged brain tissue. The M1 type of polarization is usually regarded as neurotoxic, whereas M2 is considered neuroprotective. Several studies have focused on elucidating the mechanism of M1/M2 polarization and aimed to regulate this phenotype shift to facilitate repair (Amantea and Bagetta 2016).

Apoptosis and necrosis are 2 major types of cell death occurring after cerebral ischemia. Apoptosis is usually regarded as noninflammatory, while necrosis is proinflammatory because it releases damage-associated molecules, such as HMGB1, that trigger inflammation (Scaffidi et al. 2002). For a long time, necrosis was thought to be uncontrollable. Recently, a type of programmed necrosis, named necroptosis, has been defined, and the corresponding molecular mechanism been gradually revealed (Degterev et al. 2005; Sun and Wang 2014). Upon stimulation of death signals, in cases where apoptotic signaling is inhibited, cells upregulate levels of receptor interacting protein kinase 1 (RIPK1) and receptor interacting protein kinase 3 (RIPK3), which activate a signaling cascade involving phosphorylation of the mixed lineage kinase domain-like protein (MLKL) and result in necrosis of the cell (Christofferson and Yuan 2010; Grootjans et al. 2017; Weinlich et al. 2017). Interestingly, necroptotic cells not only release damage-associated molecular patterns (DAMP) but also upregulate inflammatory cytokines, indicating an active role in the regulation of inflammation (Murakami et al. 2014; Chan et al. 2015; Wallach et al. 2016). Although early studies in necroptosis have involved ischemic stroke (Degterev et al. 2005), and later studies reported that p53-mediated programmed necrosis also contributes to the neuronal loss following ischemia (Vaseva et al. 2012), it is still unknown whether necroptotic neural cells regulate the M1/2 polarization of microglia/macrophages.

In the present study, we addressed this question by analyzing the cellular type of necroptosis in wild-type (WT) animals and investigating microglia/macrophage activation in RIPK3$^{-/-}$ and MLKL$^{-/-}$ mice. Our data demonstrated that necroptotic neurons play a crucial role in modulating M1/M2 polarization of microglia/macrophages, possibly through Myd88 signaling.

Materials and Methods

Photochemical Ischemia and Mice Treatment

Focal cortical ischemia was induced by photothrombosis of the cortical microvessels as described (Lee et al. 2007). Rose bengal (Sigma) was injected through the tail vein at a concentration of 20–25 mg/kg. A skull window was carefully made without hurting the brain tissue. The brain was illuminated for 10 min using a cold light source (Zeiss FL1500 LCD).

For behavioral tests, the skull widow was made 0.3–2.3 mm anterior to the Bregma and 0.5–3.0 mm right of the midline. Behavioral tests were performed at 1, 3, 7, and 14 dpi.

For interfering with Myd88 signaling, Myd88 inhibitory peptide (MIP, R & D system) was administered i.p. at 10 mg/kg per day from 3 to 6 dpi.

For *in vivo* propidium iodide (PI) staining, 20 mg/kg of PI in a total volume of not more than 100 μL was administered (i.p.) to mice 1 h before sacrifice as described (Fan et al. 2015, 2016).

Immunohistochemistry and H.E. Staining

For immunohistochemistry, mice were perfused intracardially with 4% paraformaldehyde phosphate buffer. Serial coronal sections were prepared. Slides were blocked using PBS containing 0.3% Triton X-100 and 3% BSA, and incubated with primary antibodies (detailed information provided in Supplementary Information) overnight at room temperature. Corresponding secondary antibodies conjugated with Alexa Fluor 594 (donkey antimouse, anti-rabbit, or anti-goat IgG, 1:800, Jackson ImmunoResearch), Alexa Fluor 488 (donkey anti-rabbit or donkey anti-goat IgG, 1:500, Jackson ImmunoResearch), and Alexa Fluor 647 (donkey anti-rabbit IgG, 1:1000, Jackson ImmunoResearch) were incubated with the sections for 2–4 h at room temperature protected from light.

For TUNEL/NeuN double-staining, TUNEL staining was performed first according to the manual of DeadEND^{TM} TUNEL system (Promega), and then followed by immunostaining of NeuN.

For H.E. staining, sections were incubated with Hematoxylin for 5 min, rinsed with tap water, and blued by 1% ammonia water. Sections were then mordanted using 95% ethanol and stained with Eosin for 10 min. Graded dehydration was finally performed, and coverslips were mounted for observation.

Immunoelectron microscopy

The immune-electron microscopic study was performed as described (Wang et al. 2006). Briefly, at 3 or 7 dpi, mice were perfusion-fixed with a mixture of 4% paraformaldehyde, 0.05% glutaraldehyde, and 15% saturated picric acid for 30 min. Next, the cortex was removed and postfixed in the same fixative without glutaraldehyde for 3 h. Tissue sections were prepared using a vibratome. Following one freeze–thaw treatment, the sections were blocked using 5% bovine serum albumin and 5% normal goat serum and then sequentially incubated with anti-MLKL antibody and goat anti-rat IgG conjugated to 1.4 nm gold particles (1:100, Nanoprobes), overnight at room temperature. After rinsing, the sections were postfixed with 2% glutaraldehyde. Silver enhancement was performed with an HQ Silver Kit (Nanoprobes). Sections were further fixed with 0.5% osmium tetroxide, dehydrated with graded ethanol, replaced with propylene oxide, and flat-embedded in Epon 812. Ischemic regions were selected, trimmed under a stereomicroscope and mounted for ultrathin sectioning. Ultrathin sections (70–80 nm)

were prepared on an LKB Nova Ultratome. After being counterstained with uranyl acetate and lead citrate, the sections were examined under an electron microscope (JEM-1230).

Primary Cell Culture and Treatments

For the culture of primary cortical neurons, brains of E15–E17 mouse embryos were removed under a stereomicroscope. The cortex was dissected and digested in 0.125% trypsin for 10 min at 37 °C. Neurons were cultured in Neurobasal medium supplemented with 2% B27 and 1% N2 for 5–6 days.

For the culture of primary cortical astrocytes, primary cells were isolated from the cortices of P2-4 neonatal pups and cultured in DMEM containing 10% fetal bovine serum. Astrocytes were purified as described, with modifications (Hamby et al. 2006; Gingras et al. 2007). Briefly, when cells reached confluence, the culture was purified by shaking at 260 rpm overnight, and the suspended microglia and oligodendrocytes were discarded. The cells were then cultured with 8 μM of arabinoside C (Ara C) for 3 days, followed by a 1-h L-leucine methyl ester (LME, 60 μM) treatment. The cell shaking, passaging, Ara C and LME treatment were repeated once to ensure that 99% of the cells used for experiments were GFAP-positive.

For the culture of microglia, primarily cultured astrocytes were shaken at 260 rpm for 30 min. The cells in the suspension were collected and replated. The purity of microglia was confirmed by immunostaining of Iba-1.

For the culture of macrophages, bone marrow cells were collected from the femurs and tibias of mice by trituration using 26-gauge needles. Red blood cells were lysed by lysis buffer before washing with DMEM. Cells were cultured in DMEM supplemented with 10% FBS and 10–30 ng/mL of macrophage colony-stimulating factor (M-CSF). After 7–10 days of culture, nonadherent cells were removed.

For oxygen-glucose deprivation (OGD), neurons and astrocytes were cultured with glucose-free DMEM in a hypoxic chamber (95% N_2 and 5% CO_2) at 37 °C for 2 and 4 h, respectively. Twenty-four hours after OGD, the conditioned medium (CM) and dying cells were collected for further experiments.

For the polarization study of macrophages *in vitro*, adherent cells were treated with CM from control WT or RIPK3$^{-/-}$ neurons and OGD-treated WT or RIPK3$^{-/-}$ neurons. Forty-eight hours later, the CM was removed, and macrophages were collected for analysis.

For interfering with Myd88 signaling, MIP or control peptide (CP) was added at a final concentration of 100 μM.

Flow-Cytometry Analysis

Periphery blood was collected from WT, RIPK3$^{-/-}$ and MLKL$^{-/-}$ mice. After discarding lymphocytes and monocytes, single-cell suspension was made and blocked with 25% rat serum for 20 min. Cells were incubated with rat anti-mouse CD11b-FITC (1:100, ebioscience), rat anti-mouse CD86-APC (1:100, ebioscience) and rat anti-mouse CD206-PE (1:100, ebioscience) on ice for 30 min. After washing with PBS containing 2% FBS, cells were analyzed by Millipore flow cytometer (Guawa 6HT) with Flow Jo software version 7.6.2 (Tree Star, Ashland, OR, USA).

Western Blotting

Cortical tissues or cells were homogenized in RIPA lysis buffer. After SDS-PAGE and protein transfer, membranes were incubated with primary antibodies (detailed information provided in Supplementary Information) overnight at 4 °C, followed by incubation with HRP-conjugated anti-rabbit or anti-mouse IgG (1:5000; Proteintech) for 1 h at room temperature. Bands were visualized with an ECL kit (Thermo).

Real-Time RT-PCR

Total RNA was extracted from cortical tissues at 7 dpi, or macrophages 48 h post-treatment with OGD CM. After reverse transcription, real-time RT-PCR was carried out. mRNA levels of target genes were normalized to the mRNA levels of *Gapdh* using the ΔCt method. The detailed primer information for individual genes is included in the Supplementary Information.

Behavioral Tests

Glass sliding and footfault tests were used to assess the asymmetry in forelimb use as described (Baskin et al. 2003; Sweetnam et al. 2012). Animals were videotaped in a transparent glass cylinder for 10 min. Two mirrors combined at an angle of 90° were placed behind the glass cylinder to allow the recording of forelimb movements when the animal turned away from the camera. The numbers of contacts and the numbers of sliding movements of each forelimb at the wall of the cylinder for every spontaneous stand-up were scored. Forelimb activity (FLA) was evaluated using the following formula. FLA = (first contact + horizontal + vertical)/number of rearings. Percentages of sliding were calculated by number of sliding movements/(number of contacts + number of sliding movements) × 100. The asymmetry index was derived by subtracting the % of ipsilateral sliding from the % of contralateral sliding.

For the footfault test, a camera was placed underneath a horizontally placed ladder (1.5 cm wide between the rungs) to assess the animals' stepping errors (i.e., "footfaults"). Animals were given 10 min to walk atop the elevated wire surface. A step was considered a footfault if it was not providing support or a slip/miss occurred. Footfaults for each limb were counted and compared with the overall number of steps made by that limb. Footfault scores were calculated as footfault per step/steps per limb × 100. Percentages of footfaults was calculated as number of footfaults/(number of steps+number of footfaults)×100. The asymmetry index was derived by subtracting the % of ipsilateral footfaults from the % of contralateral footfaults.

Image Collection and Statistical Analysis

All images of H.E. staining and immunofluorescent staining were taken by Olympus BX51 and Olympus FV1000, respectively. Images were analyzed by Image J or Photoshop CS 6.0. At least 3 mice for each group were used for comparison. Data were presented as the mean ± standard error. Statistical comparisons were made using Student's *t*-test or analysis of variance (ANOVA) with Student Newman–Keuls post hoc analysis. *P* value less than 0.05 was considered as statistical significant.

Results

Ischemia Induces Rapid Neuron-Dominant Necroptosis in Mice Cortex

A photothrombosis model was adopted to induce focal ischemia in the cerebral cortex of C57 mice (Yang et al. 2016). We first examined the occurrence of necrosis in the ischemic cortex by *in vivo* PI labeling (Fan et al. 2015, 2016). Starting from 24 h post-injury, plenty of PI-positive cells were observed in the

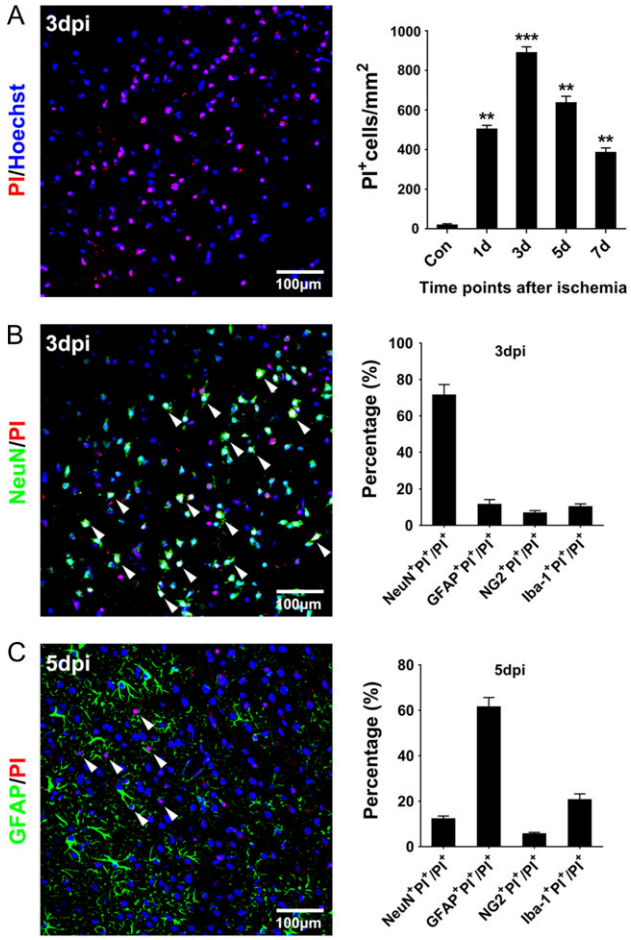

Figure 1. Cellular necrosis following ischemia. (*A*) *In vivo* PI labeling and quantification of PI-positive cells at the lesion site. The number of PI-positive cells reached a peak at 3 dpi. (*B*) Combination of immunohistochemistry of neural cell markers with PI-labeling at 3 dpi. Left panel shows the combination of NeuN-staining with PI-labeling. Right panel shows the cell type composition of PI-positive cells. (*C*) Combination of immunohistochemistry of neural cell markers with PI-labeling at 5 dpi. Left panel shows the combination of GFAP-staining with PI-labeling. Right panel shows the cell type composition of PI-positive cells. Notice that the major cell types of PI-positive cells are neurons at 3 dpi and astrocytes at 5 dpi. Arrowheads in *B* and *C* indicate double-positive cells. $N = 5$ mice per group. $^{**}P < 0.01$ compared with control group. $^{***}P < 0.001$ compared with control group.

infarction area, and their numbers peaked at 3 days post-injury (dpi) (Fig. 1A). Combined immunostaining of different neural cell markers with PI demonstrated that at 3 dpi, approximately 71.4 ± 5.8% of the PI-labeled cells were NeuN-positive (Fig. 1B). From 5 dpi onward, the number of PI-labeled cells decreased and cell types labeled with PI changed (Fig. 1B). At 5 dpi, most of the PI-positive cells were GFAP-positive (Fig. 1C). These data indicated that after focal cerebral ischemia, there is a rapid neuron-dominant necrosis followed by an astrocyte-dominant necrosis in the later phase.

To explore whether necroptosis contributes to ischemia-induced necrosis, we next examined the expression of RIPK3, MLKL and phosphorylated MLKL (pMLKL) in the ischemic cortex. Western blotting demonstrated that RIPK3, MLKL and pMLKL were upregulated at 24 h postischemia, and this upregulation persisted through 7 dpi (Fig. 2A). Consistent with PI-labeling, at 3 dpi, most of the pMLKL-positive cells were NeuN-positive (Fig. 2B). At 5 dpi, GFAP-positive astrocytes made up most of the pMLKL-positive cells in the ischemic cortex (Fig. 2C). To confirm the occurrence of necroptosis, we performed immune-electron microscopic study y of MLKL. At 3 dpi, nanogold labeled MLKL immunoreactivities were observed to be enriched in cells showing lysis of the cytoplasmic content and ultrastructural features of neurons (Fig. 2D). At 5 dpi, most MLKL immunoreactivities were observed in cells with lysis of the cytoplasmic content and glial fibers (Fig. 2E). These data indicated that neuronal necroptosis occurs in the acute phase after ischemia, and in the later phase, astrocytes also undergo RIPK3/MLKL-mediated necroptosis.

Inhibition of Necroptosis Alleviates Injury and Facilitates Functional Recovery

We next performed photothrombosis in the cortex of RIPK3$^{-/-}$ and MLKL$^{-/-}$ mice and measured infarction size at 7 and 14 dpi, respectively. The results demonstrated that compared with WT mice, there was significant reduction in lesion size in the cortex of RIPK3$^{-/-}$ mice by approximately 29% at 7 dpi and approximately 45% at 14 dpi (Fig. 3A,B). Similarly, MLKL$^{-/-}$ mice showed a significant decrease in lesion size by approximately 30% at 7 dpi and 48% at 14 dpi (Fig. 3A,B), suggesting a role of necroptosis in lesion development in ischemia. Further analysis showed that, at 7 dpi, there was significantly less number of TUNEL/NeuN-positive cells in the cortex of RIPK3$^{-/-}$ and MLKL$^{-/-}$ mice (Fig. 3C). Interestingly, more hematoxylin-stained inflammatory cells were observed in the ischemic regions of RIPK3$^{-/-}$ and MLKL$^{-/-}$ cortices than those in the WT cortex at 7 dpi and these cells diminished at 14 dpi (Fig. 3A,B).

To evaluate whether blocking necroptosis helped functional recovery following ischemia, we induced ischemia in the sensorimotor cortex and performed FLA assays and footfault assays to assess the recovery of forelimb locomotion. Following ischemia, forelimb activities reduced immediately to approximately <40% of baseline in WT, RIPK3$^{-/-}$ and MLKL$^{-/-}$ mice (Fig. 3D). From 7 dpi onward, significant recovery of forelimb locomotion was observed in both RIPK3$^{-/-}$ and MLKL$^{-/-}$ mice compared with WT controls, as indicated by the increase in forelimb activities and reduction of sliding movements (Fig. 3D,E). The footfault assay demonstrated that ischemia quickly resulted in obvious stepping faults in all mice. A significant decrease in footfault steps and reduction in the asymmetric index was observed in RIPK3$^{-/-}$ and MLKL$^{-/-}$ mice from 7 dpi onwards (Fig. 3F,G). These data suggested that blocking necroptosis reduced tissue damage and was helpful in functional recovery.

Defective Necroptosis Induces Polarization Bias in Macrophages/Microglia Toward M2 Phenotype in the Ischemic Cortex

As we have noticed, there seems to be more inflammatory cells in both RIPK3$^{-/-}$ and MLKL$^{-/-}$ cortices at 7 dpi (Fig. 3A). Since the microglia/macrophage-mediated innate immune response is the predominant immune reaction in the brain, we first examined the expression of Iba-1—a marker of microglia/macrophages—by immunohistochemistry and Western blotting. In the WT cortex, Iba-1-positive cells were distributed primarily surrounding the infarction core, while in both RIPK3 and MLKL-deficient cortices, Iba-1-positive cells filled the infarction core as well as the surrounding region (Fig. 4A). No significant increase of Iba-1-positive cells was observed in the contralateral cortex of RIPK3$^{-/-}$ and MLKL$^{-/-}$ mice, compared with that in WT mice (Fig. 4A). Western blotting confirmed this increase

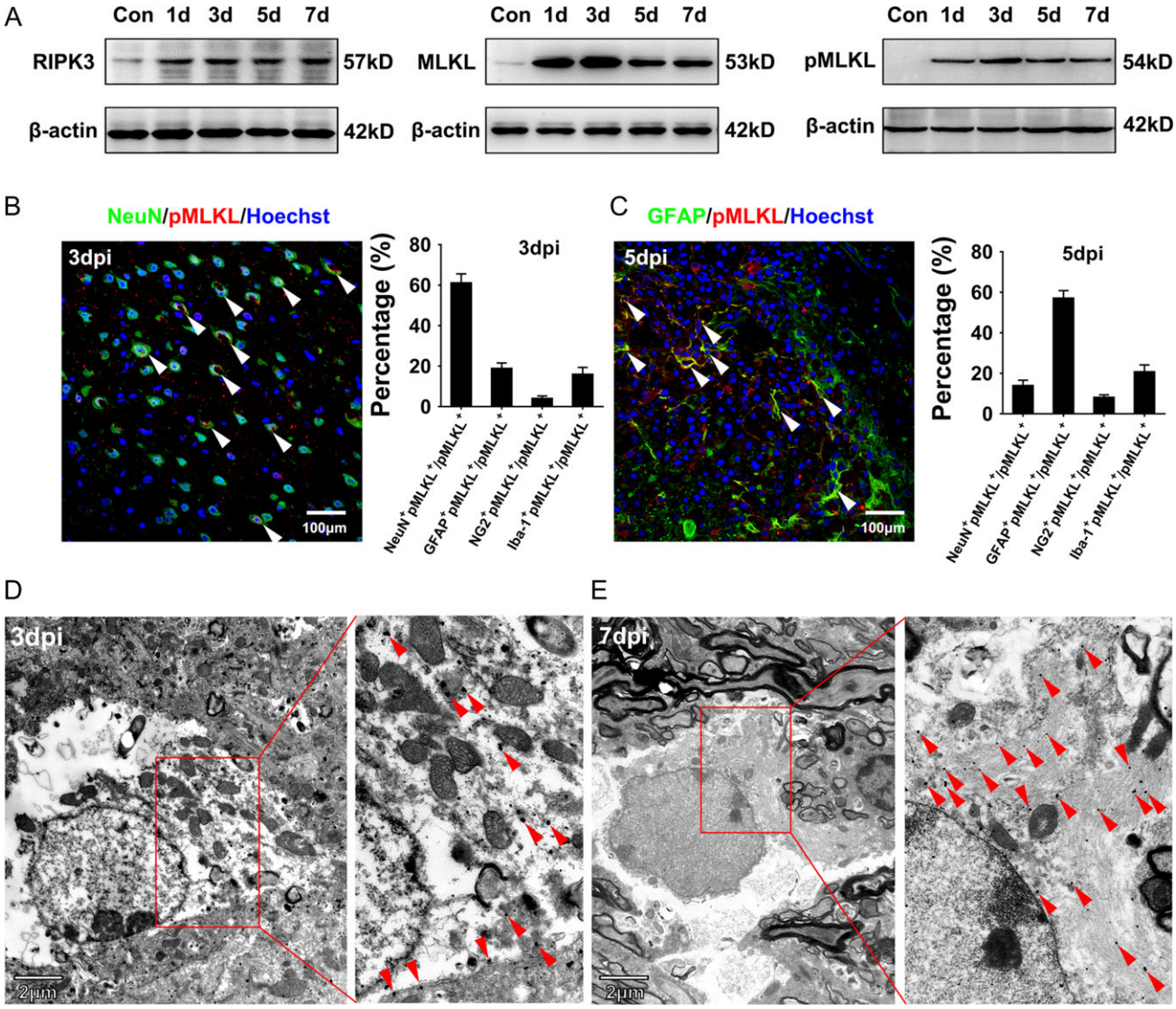

Figure 2. Cellular necroptosis in the ischemic cortex. (*A*) Western blotting of RIPK3, MLKL and pMLKL in the ischemic cortex. (*B*) Double-immunostaining of pMLKL with neural cell markers and quantification at 3 dpi. Left panel: representative image of NeuN/pMLKL-staining. *Right panel*: quantification of cell type composition of pMLKL-positive cells. (*C*) Double-immunostaining of pMLKL with neural cell markers and quantification at 5 dpi. *Left panel*: representative image of GFAP/pMLKL-immunostaining. *Right panel*: quantification of cell type composition of pMLKL-positive cells. Notice that the major cell types of pMLKL-positive cells are neurons at 3 dpi and astrocytes at 5 dpi. (*D*, *E*) Immunoelectron microscopic (EM) study of MLKL at 3 dpi (*D*) and 5 dpi (*E*). Notice MLKL-positive neurons at 3 dpi and MLKL-positive astrocytes at 5 dpi with lysis of cytoplasm. Arrowheads in *D* and *E* indicate MLKL-positive nanogold particles.

of Iba-1 expression in the ischemic RIPK3- and MLKL-deficient cortices (Fig. 4B, Supplementary Fig. S1A, B).

Considering that there are primarily 2 types of activated microglia/macrophages, namely, M1 and M2, which exhibit distinct functions (Hu et al. 2015), we next examined the expression of M1 markers and related cytokines. Immunohistochemistry demonstrated that in uninjured WT, RIPK3$^{-/-}$ and MLKL$^{-/-}$ cortices, there were few iNOS/F480-positive cells (Fig. 4C, upper panel). At 7 dpi, strong iNOS immunoreactivities were detected, primarily overlapping with F4/80-positive cells in the ischemic cortex. In RIPK3$^{-/-}$ and MLKL$^{-/-}$ mice, the number of F4/80-positive cells expressing iNOS significantly reduced at 7 dpi (Fig. 4C, lower panel). Western blotting confirmed this upregulation of iNOS by ischemia in the WT cortex and the compromised upregulation of iNOS in RIPK3$^{-/-}$ and MLKL$^{-/-}$ mice (Fig. 4D, Supplementary Fig. S1C, D). Furthermore, real-time RT-PCR demonstrated that the mRNAs of iNOS and proinflammatory factors TNFα, IL-12 and IL-18 were all compromised in both the RIPK3$^{-/-}$ and MLKL$^{-/-}$ cortices, compared with those observed in WT controls (Fig. 4E,F). These data indicated that blocking necroptosis attenuates M1 polarization of microglia/macrophages in the ischemic cortex.

We next examined the expression of the M2 phenotype-associated markers and cytokines. Immunohistochemistry demonstrated that in the uninjured cortices of WT, RIPK3$^{-/-}$ and MLKL$^{-/-}$ mice, there were few Arginase-1 (Arg-1)-positive cells (Fig. 5A, upper panel). At 7 dpi, there was a moderate increase in Arg-1-immunoreactivities in the Iba-1-positive cells in the WT cortex (Fig. 5A, lower panel). Stronger Arg-1-immunoreactivities were observed in the ischemic cortices of RIPK3$^{-/-}$ and MLKL$^{-/-}$ mice (Fig. 5A, lower panel). Western blotting and real-time RT-PCR confirmed the upregulation of Arg-1 in the ischemic RIPK3$^{-/-}$

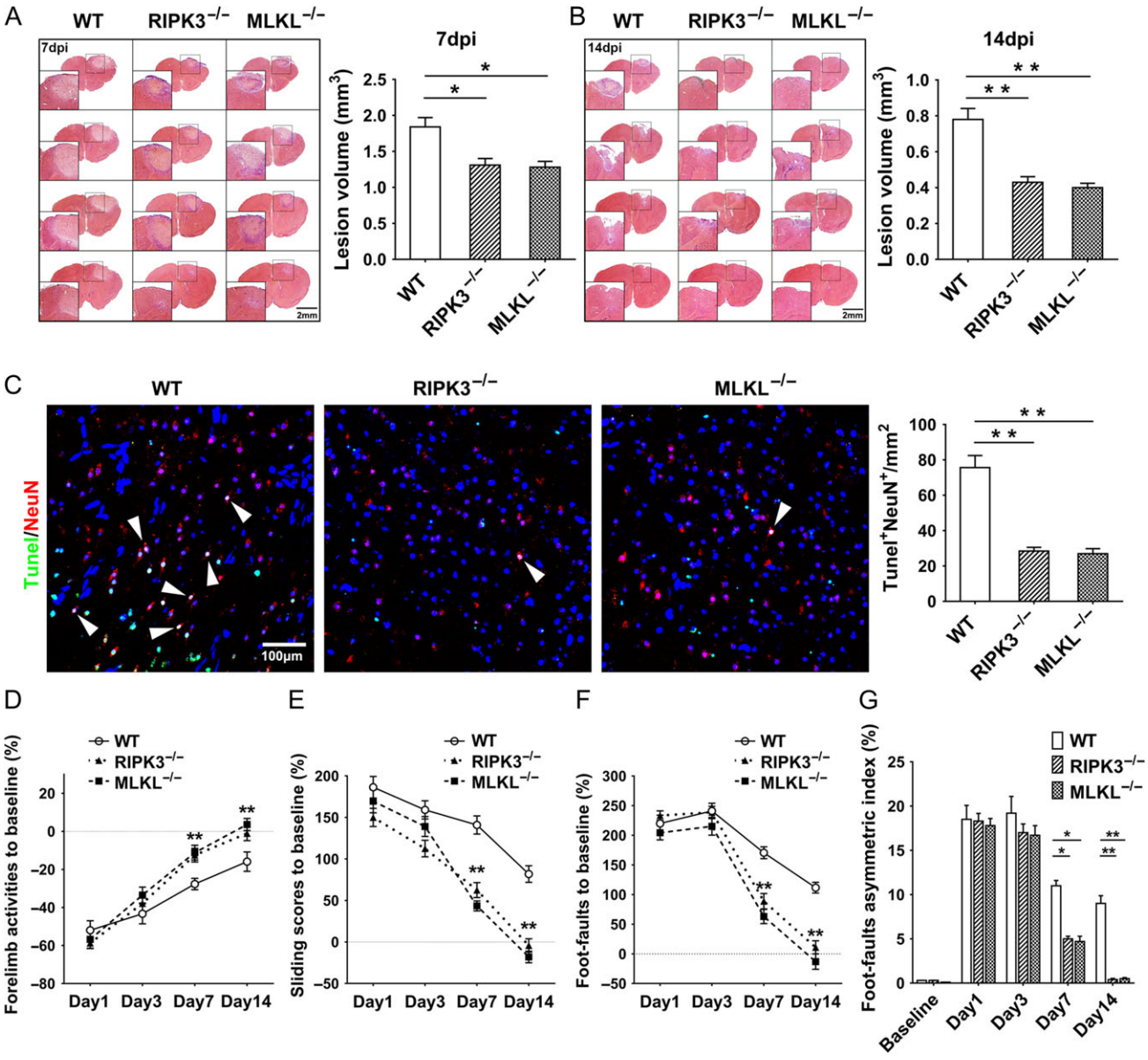

Figure 3. Effects of RIPK3- and MLKL-deficiency on lesion size and locomotion recovery. (*A*, *B*) Effects of RIPK3- and MLKL-deficiency on lesion size at 7 dpi (*A*) and 14 dpi (*B*), respectively. Notice the smaller lesion area in both RIPK3$^{-/-}$ and MLKL$^{-/-}$ cortices. *N* = 8 mice in each group. Inserts are magnified lesion region. Notice the blue-stained inflammatory cells. (*C*) Combination of TUNEL staining with immunohistochemistry of NeuN at 7 dpi in WT, RIPK3$^{-/-}$ and MLKL$^{-/-}$ mice. Notice the less number of TUNEL/NeuN-positive cells in RIPK3$^{-/-}$ and MLKL$^{-/-}$ cortices. (*D*, *E*) Spontaneous forelimb activity assays of WT, RIPK3$^{-/-}$ and MLKL$^{-/-}$ mice following ischemia. *N* = 6 mice in each group. (*F*, *G*) Footfault assays of WT, RIPK3$^{-/-}$ and MLKL$^{-/-}$ mice following ischemia. *N* = 6 mice in each group. Notice that RIPK3$^{-/-}$ and MLKL$^{-/-}$ mice showed better locomotion recovery from 7 dpi onward. Arrowheads in C indicate double-positive cells. *P < 0.05. **P < 0.01.

and MLKL$^{-/-}$ cortices (Fig. 5B,C, and Supplementary Fig. S1E, F), suggesting that inhibiting necroptosis biased microglia/macrophages toward an M2 fate. In line with this observation, significant increases in anti-inflammatory factors IL-4 and IL-10 were detected by real-time RT-PCR in both RIPK3$^{-/-}$ and MLKL$^{-/-}$ cortices at 7 dpi, compared with the levels observed in WT controls (Fig. 5D).

The no changes of iNOS and Arg-1 in the contralateral cortex of ischemic injury excluded a role of RIPK3 and MLKL in naïve microglia. To explore the effects of RIPK3- and MLKL-deficiency on blood macrophages, we performed flow cytometry analysis. The expression of M2 marker CD206 in CD11b-positive cells were similar among WT, RIPK3$^{-/-}$ and MLKL$^{-/-}$ mice. The expression of M1 marker CD86 in CD11b-positive cells of RIPK3$^{-/-}$ and MLKL$^{-/-}$ mice was even higher than that in WT mice (Supplementary Fig. S2A). These data excluded the M2-inducing effect of RIPK3- and MLKL-deficiency on naïve macrophages. Further, we tested whether the switch of M1/M2 microglia/macrophages in ischemic cortex was related to apoptosis by examining polarization in Caspase-3$^{-/-}$ mice. Western blotting showed a moderate upregulation of iNOS but no change of Arg-1 in the ischemic cortex of Caspase-3$^{-/-}$ mice (Supplementary Fig. S2B,C). Taken together, these data indicated that necroptosis may play an important role in regulating the M1/M2 polarization of microglia/macrophages in the ischemic cortex.

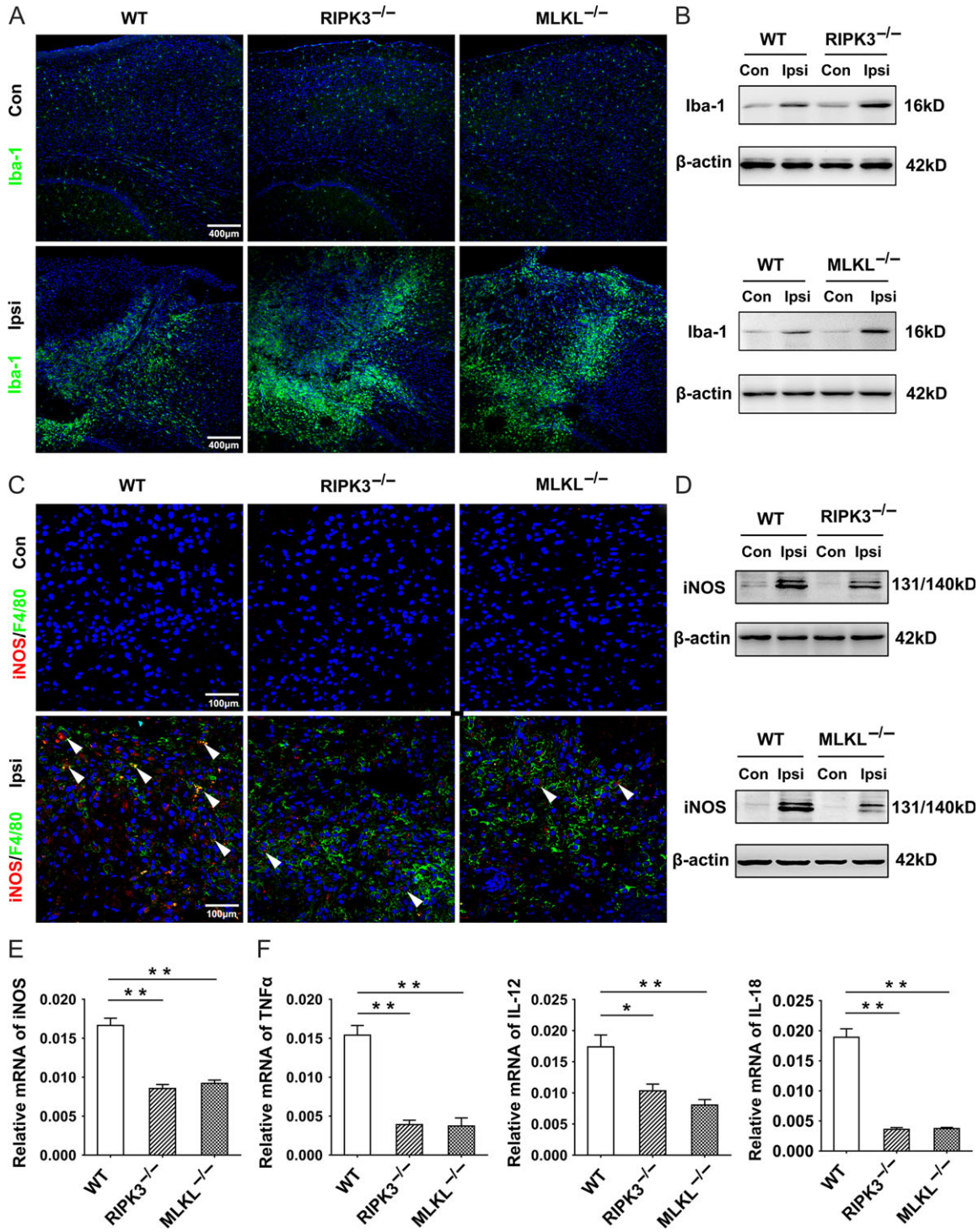

Figure 4. RIPK3- and MLKL-knockout attenuate M1 polarization of microglia/macrophages in the ischemic cortex. (*A*, *B*) Immunostaining and Western blotting of Iba-1 in the contralateral (Con) and ipsilateral cortex (Ipsi) of WT, RIPK3$^{-/-}$, MLKL$^{-/-}$ mice at 7 dpi. Notice the increase of Iba-1 in the ischemic cortex of RIPK3$^{-/-}$, MLKL$^{-/-}$ mice compared with that in WT mice. (*C*) Double-immunostaining of iNOS with F4/80 in the contralateral (Con) and ipsilateral cortex (Ipsi) of WT, RIPK3$^{-/-}$, MLKL$^{-/-}$ mice at 7 dpi. (*D*) Western blotting of iNOS in the contralateral (Con) and ipsilateral cortex (Ipsi) of WT, RIPK3$^{-/-}$, MLKL$^{-/-}$ mice at 7 dpi. (*E*, *F*) Real-time RT-PCR of iNOS (*E*), TNFα, IL-12 and IL-18 (*F*) in the ischemic cortex of WT, RIPK3$^{-/-}$, MLKL$^{-/-}$ mice at 7 dpi. Notice the relatively lower expression of iNOS, TNFα, IL-12 and IL-18 in the ischemic cortices of RIPK3$^{-/-}$ and MLKL$^{-/-}$ mice compared with that in WT mice. Arrowheads in C indicate double-positive cells. $N = 3$ mice in each group. *$P < 0.05$. **$P < 0.01$.

Since M2 microglia/macrophages have been supposed to be neuroprotective (Xiong et al. 2016; Ma et al. 2017), we next investigated the effects of RIPK3- or MLKL-deficiency on the expression of neurotrophic factor in microglia/macrophages. Double-immunostaining showed that there were more Iba-1-positive cells expressing brain-derived neurotrophic factor (BDNF, Fig. 5E). Western blotting confirmed the higher expression of BDNF in the ischemic cortex of RIPK3$^{-/-}$ and MLKL$^{-/-}$

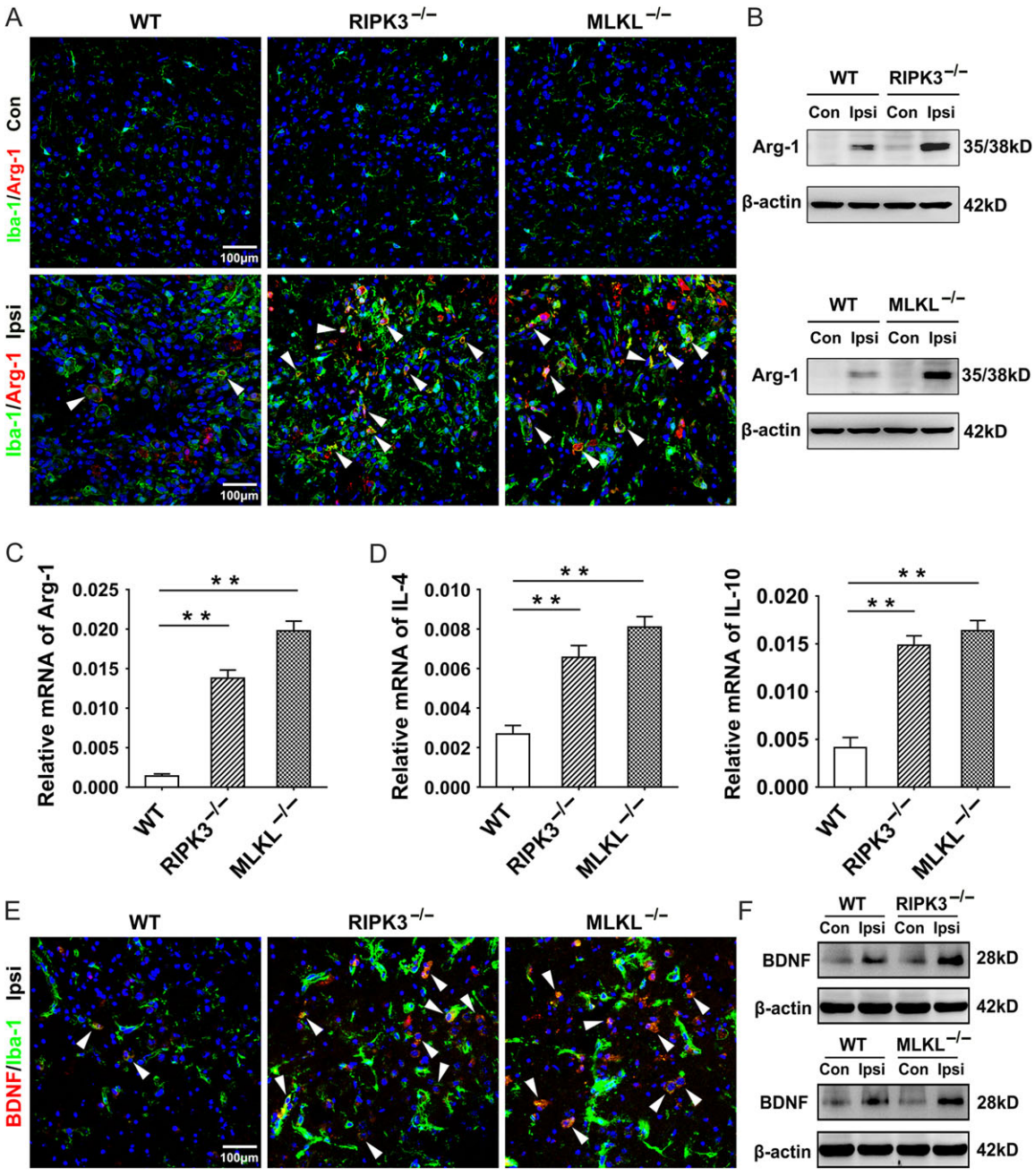

Figure 5. RIPK3- and MLKL-knockout promote M2 polarization of microglia/macrophages in the ischemic cortex. (*A*) Double-immunostaining of Arg-1 with Iba-1 in the contralateral (Con) and ipsilateral cortex (Ipsi) of WT, RIPK3$^{-/-}$, MLKL$^{-/-}$ mice at 7 dpi. (*B*) Western blotting of Arg-1 in the contralateral (Con) and ipsilateral cortex (Ipsi) of WT, RIPK3$^{-/-}$, MLKL$^{-/-}$ mice at 7 dpi. (*C*, *D*) Real-time RT-PCR of Arg-1 (*C*), IL-4 and IL-10 (*D*) in the ischemic cortex of WT, RIPK3$^{-/-}$, MLKL$^{-/-}$ mice at 7 dpi. Notice the relatively higher expression of Arg-1, IL-4, and IL-10 in the ischemic cortices of RIPK3$^{-/-}$ and MLKL$^{-/-}$ mice compared with that in WT mice. (*E*) Double-immunostaining of BDNF with Iba-1 in the ipsilateral cortex (Ipsi) of WT, RIPK3$^{-/-}$, MLKL$^{-/-}$ mice at 7 dpi. (*F*) Western blotting of BDNF in the contralateral (Con) and ipsilateral cortex (Ipsi) of WT, RIPK3$^{-/-}$, MLKL$^{-/-}$ mice at 7 dpi. $N = 3$ mice in each group. $^{**}P < 0.01$. Arrowheads in *A* and *E* indicate double-positive cells.

mice at 7 dpi (Fig. 5F, Supplementary Fig. 3A, 3B). These data indicated that blocking necroptosis might enhance the neuroprotective phenotype of microglia/macrophages.

Necroptotic Neurons Polarize Macrophages Toward M1 Phenotype in Vitro

Since neurons and astrocytes are the 2 major cell types that undergo necroptosis following ischemia, we next investigated whether necroptotic neurons or astrocytes modulated the polarization of microglia/macrophages *in vitro*. Primary neurons and astrocytes were subjected to oxygen and glucose deprivation (OGD), and the CM was collected to stimulate primary microglia/macrophages. Necroptosis of OGD-treated neurons and astrocytes was confirmed by Western blotting of RIPK3 and pMLKL (Supplementary Fig. S4A–D). Stimulating primary microglia with CM of OGD-treated neurons resulted in significant upregulation of iNOS (Supplementary Fig. S4E), suggesting a role

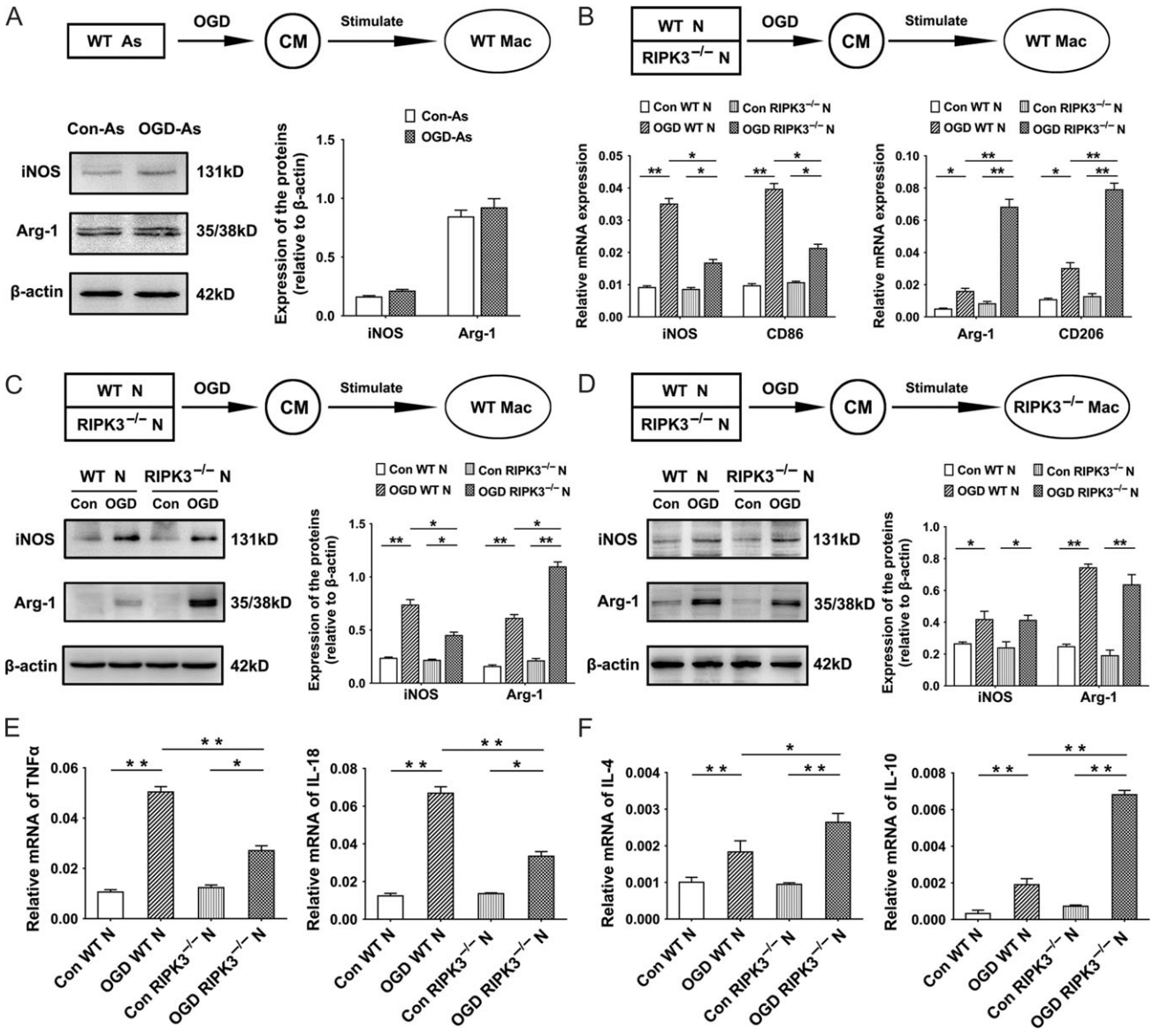

Figure 6. Necroptotic neurons induce M1 polarization of macrophages *in vitro*. (*A*) Experimental design, and Western blotting of iNOS and Arg-1 in macrophages treated with the CM of control astrocytes (Con-As) and OGD-treated astrocytes (OGD-As). No significant changes in iNOS and Arg-1 were detected. (*B*) Experimental design, and real-time RT-PCR of iNOS, CD86, Arg-1 and CD206 in macrophages treated with the CM of control WT neurons (Con WT N), OGD-treated WT neurons (OGD WT N), control RIPK3$^{-/-}$ neurons (Con RIPK3$^{-/-}$ N), and OGD-treated RIPK3$^{-/-}$ neurons (OGD RIPK3$^{-/-}$ N). Notice that the CM of OGD-treated WT neurons induced relatively higher levels of M1 markers (iNOS, CD86), while the CM of OGD-treated RIPK3$^{-/-}$ neurons led to higher expression of M2 markers (Arg-1, CD206) in WT macrophages. (*C*) Experimental design, and Western blotting of iNOS and Arg-1 in WT macrophages treated with different CM as above. (*D*) Experimental design, and Western blotting of iNOS and Arg-1 in RIPK3$^{-/-}$ macrophages treated with different CM as above. (*E*, *F*) Real-time RT-PCR of TNFα, IL-18 (*E*), IL-4 and IL-10 (*F*) in control WT neurons, OGD-treated WT neurons, control RIPK3$^{-/-}$ neurons, and OGD-treated RIPK3$^{-/-}$ neurons. Notice that OGD-treated WT neurons expressed relatively higher levels of M1 cytokines (TNFα, IL-18), while the OGD-treated RIPK3$^{-/-}$ neurons expressed higher levels of M2 cytokines (IL-4 and IL-10). $N = 3$ batches of cell for each experiment. *$P < 0.05$. **$P < 0.01$.

of necroptotic neurons on the M1-polarization of microglia/macrophages. Considering the easy availibility, we next mainly used primary macrophages in the following *in vitro* study. Treatment of macrophages with CM of OGD-treated astrocytes exerted no significant effects on the expression of iNOS and Arginase-1 in primary macrophages (Fig. 6*A*). To directly investigate the effects of necroptotic neurons on the polarization of microglia/macrophages, we treated WT macrophages with the CM of normal WT neurons, OGD-treated WT neurons, normal RIPK3$^{-/-}$ neurons and OGD-treated RIPK3$^{-/-}$ neurons (Fig. 6*B*,*C*). Real-time RT-PCR demonstrated that the CM of OGD-treated WT neurons significantly increased the expression of M1 markers, iNOS and CD86, while the CM of OGD-treated RIPK3$^{-/-}$ neurons significantly increased the expression of M2 markers, Arg-1 and CD206 in WT macrophages at 48 h after treatment (Fig. 6*B*). Upregulation of iNOS by OGD-treated WT neurons and the induction of Arg-1 in WT macrophages by OGD-treated RIPK3$^{-/-}$ neurons were confirmed by Western blotting (Fig. 6*C*). We next used the above CM to stimulate RIPK3$^{-/-}$ macrophages (Fig. 6*D*). The results showed that OGD CM of WT and RIPK3$^{-/-}$ neurons induced upregulation of both iNOS and Arg-1 in RIPK3$^{-/-}$ macrophages. However, the folds of iNOS/Arg-1 upregulation in RIPK3$^{-/-}$ macrophages were

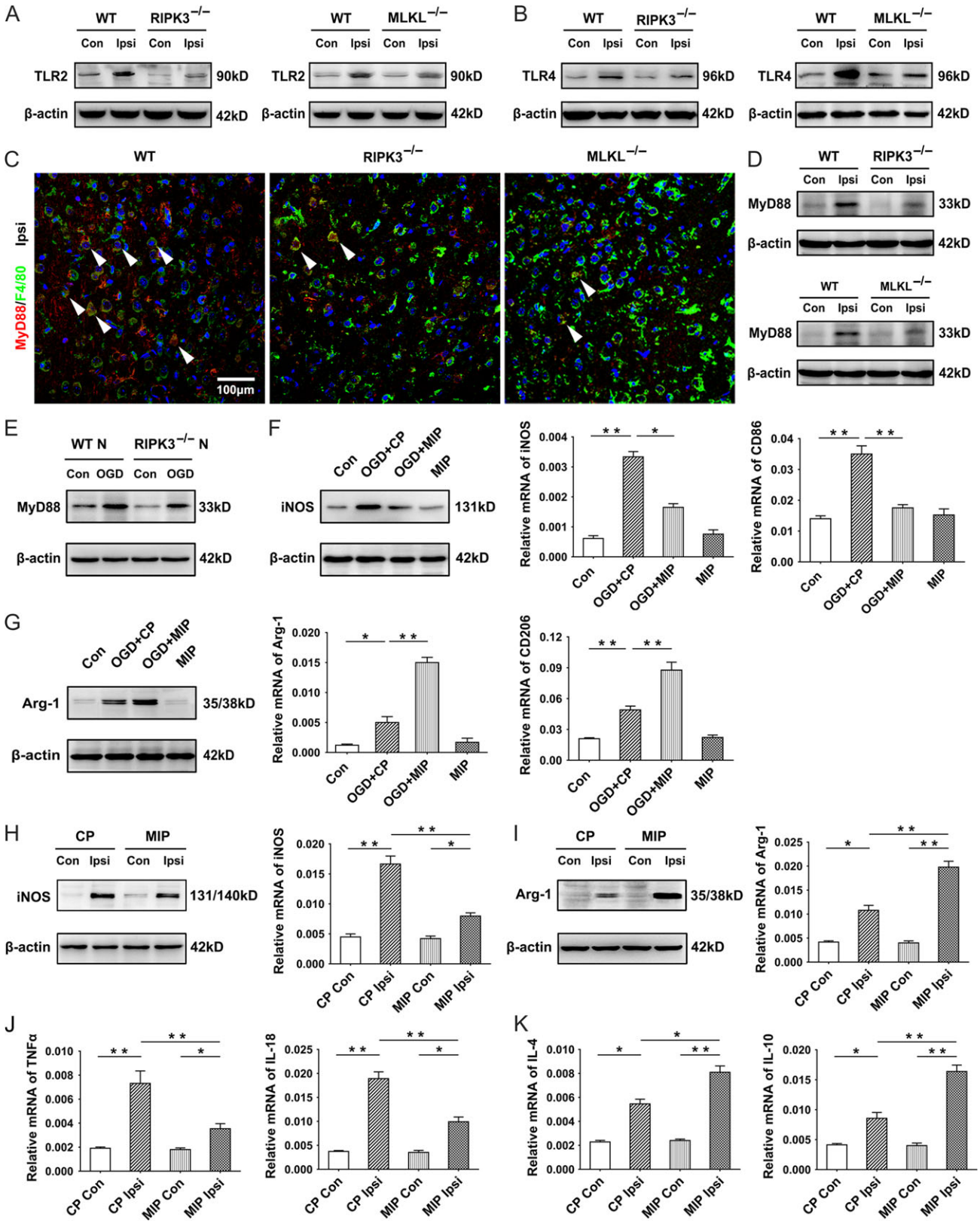

Figure 7. Myd88 mediates the effects of necroptotic neurons on the polarization of microglia/macrophages. (A) Western blotting of TLR2 in the contralateral (Con) and ipsilateral cortex (Ipsi) of WT, RIPK3$^{-/-}$, MLKL$^{-/-}$ mice at 7 dpi. (B) Western blotting of TLR4 in the contralateral (Con) and ipsilateral cortex (Ipsi) of WT, RIPK3$^{-/-}$, MLKL$^{-/-}$ mice at 7 dpi. Notice the compromised upregulation of TLR2 and TLR4 in the ischemic cortex of RIPK3$^{-/-}$ and MLKL$^{-/-}$ mice. (C, D) Immunostaining and Western blotting of Myd88 in WT, RIPK3$^{-/-}$ and MLKL$^{-/-}$ mice at 7 dpi. (E) Western blotting of Myd88 in macrophages treated with the CM of control WT neurons, OGD-treated WT neurons, control RIPK3$^{-/-}$ neurons, and OGD-treated RIPK3$^{-/-}$ neurons. (F) Western blotting of iNOS and real-time RT-PCR of iNOS and CD86 in macrophages treated with the CM of control neurons, CM of OGD-treated neurons plus control peptide (CP), CM of OGD-treated neurons plus Myd88 inhibitory peptide

similar under stimulations of OGD CM from WT neurons or RIPK3$^{-/-}$ neurons (Fig. 6D). These data indicated that the RIPK3 signaling in neurons was essential for inducing the M1-polarization of macrophages. Further analysis demonstrated that OGD treatment led to a dramatic increase in the mRNA levels of proinflammatory factors TNFa and IL-18 in necroptotic WT neurons (Fig. 6E). In contrast, remarkable upregulation of anti-inflammatory cytokines IL-4 and IL-10 was observed in OGD-treated RIPK3$^{-/-}$ neurons, compared with the levels observed in OGD-treated WT neurons or normal controls (Fig. 6F). These data indicated that necroptotic neurons may induce the M1 fate of microglia/macrophages, while necroptosis-defective neurons may favor M2 polarization by releasing distinct inflammatory factors.

Myd88 is Required for the Effects of Necroptotic Neurons on the Polarization of Microglia/Macrophages

Toll-like receptors (TLRs) are key receptors on the surface of microglia/macrophages to which most DAMP factors bind (Piccinini and Midwood 2010). Under inflammatory conditions, multiple TLRs are usually activated. To explore the mechanism of the polarization-modulating effects of necroptotic neurons, we first examined the expression of TLR2 and TLR4, 2 TLRs which were reportedly upregulated by microglia/macrophages after cerebral ischemia (Brea et al. 2011). Western blotting demonstrated that deficiency of RIPK3 and MLKL significantly blocked the upregulation of TLR2 and TLR4 in the ischemic cortex (Fig. 7A,B, Supplementary Fig. S5A, B). We then focused on Myd88, a common intracellular adaptor protein of all TLRs (Deguine and Barton 2014; Narayanan and Park 2015). Immunohistochemistry demonstrated an extremely low level of Myd88 expression in the normal cortex. Following ischemia, strong immunoreactivity of Myd88 was detected, primarily in F4/80-positive cells (Fig. 7C). In the ischemic cortex of RIPK3$^{-/-}$ and MLKL$^{-/-}$ mice, the number of F4/80-positive cells expressing Myd88 significantly decreased, as compared with those in the WT controls (Fig. 7C). Western blotting confirmed this upregulation of Myd88 induced by ischemia in WT mice and the compromised upregulation in RIPK3- and MLKL-deficient cortices (Fig. 7D, Supplementary Fig. 5C). *In vitro*, the CM of OGD-treated WT neurons significantly increased the expression of Myd88, while the CM of OGD-treated RIPK3$^{-/-}$ only exerted a moderate effect (Fig. 7E, Supplementary Fig. S5D). These data suggested that Myd88 may be involved in the effects of necroptotic neurons on macrophage/microglia polarization.

To further probe this possibility, we added a Myd88 inhibitory peptide (MIP), containing a TAT transmembrane peptide and a domain that interferes with the dimerization of Myd88, into the CM of OGD neurons when stimulating macrophages. Western blotting demonstrated that the CP had no effects on the induction of iNOS by the CM of OGD neurons, while MIP significantly reduced the increase of iNOS (Fig. 7F, left panel; Supplementary Fig. S5E). Real-time RT-PCR also demonstrated that MIP significantly blocked the induction of iNOS and another M1 marker, CD86, by OGD neurons (Fig. 7F, right panel). With regard to M2 markers, MIP treatment resulted in higher expression of Arg-1 as well as another M2 marker, CD206, at both the protein and mRNA levels (Fig. 7G, Supplementary Fig. S5F). These data indicated that inhibiting Myd88 may exert a similar effect as RIPK3$^{-/-}$ and MLKL$^{-/-}$ on the polarization of microglia/macrophages in the ischemic cortex.

To test this possibility *in vivo*, we injected MIP i.p. once per day from 3 to 6 dpi and examined the polarization of microglia/macrophages at 7 dpi. The results demonstrated that compared with mice treated with the CP, MIP-treated mice showed significantly lower levels of iNOS in the ischemic cortex (Fig. 7H, Supplementary Fig. S5G). Regarding M2 markers, mice treated with MIP showed significantly higher levels of Arg-1 in the ischemic cortex (Fig. 7I, Supplementary Fig. S5H). In addition, MIP suppressed the induction of proinflammatory factors TNFα and IL-18 (Fig. 7J) and promoted the expression of anti-inflammatory factors IL-4 and IL-10 (Fig. 7K). These data indicated a M2 polarizing effect of MIP treatment. In line with these results, MIP treatment significantly reduced the number of TUNEL/NeuN-positive cells and increased the expression of BDNF in microglia/macrophages in the ischemic cortex (Supplementary Fig. S5I–K). Taken together, these data indicated that Myd88 signaling may be a key intracellular signaling which mediates the effects of necroptotic neurons on the polarization of microglia/macrophages.

Discussion

In the present study, we first analyzed the time course and cell types involved in necroptosis in the murine cortex following ischemia, by *in vivo* PI-labeling, immunohistochemistry of RIPK3 and pMLKL, and immunoelectron microscopic studies. Next, we assessed the effects of necroptosis on M1/2 polarization of microglia/macrophages by Western blotting and real-time RT-PCR and further demonstrated that it was necroptotic neurons, but not necroptotic astrocytes, that induce M1 polarization of macrophages at the lesion site. Finally, our data demonstrated that Myd88 signaling in microglia/macrophages mediates the effects of necroptotic neurons on the fate switching of microglia/macrophages.

Previous studies have reported the occurrence of necroptosis and ferroptosis in the ischemic cortex and that RIPK1—a molecule upstream of RIPK3 and MLKL—contributes to neuronal and astrocytic death (Ni et al. 2017). Recent studies also reported the occurrence of necroptosis in the ischemic cortex (Yang, Lv, et al. 2017; Yang, Hu, et al. 2017; Yang, Yi et al. 2017). However, the detailed time course and cell types involved in necroptosis elicited by ischemia have not been fully analyzed. In the present study, by examining the expression of RIPK3 and MLKL, we observed that a neuron-dominant necroptosis occurs in the first 3 days after ischemia. From 5 dpi onward, the major cell types, which undergo necroptosis, changed to astrocytes. This time-dependent switch of neuron-to-astrocyte necroptosis reflects the pathological changes of cerebral ischemia and may contribute to the development of secondary injury. Acute oxidative stress and energy deprivation may account for the rapid death of neurons. P53 has been reported to contribute to the

(MIP), and MIP. (G) Western blotting of Arg-1 and real-time RT-PCR of Arg-1 and CD206 in macrophages treated with the CM of control neurons, CM of OGD-treated neurons plus control peptide (CP), CM of OGD-treated neurons plus Myd88 inhibitory peptide (MIP), and MIP. Notice that MIP treatment blocked the effects of the CM of OGD-treated neurons on the polarization of macrophages *in vitro*. (H) Western blotting and real-time RT-PCR of iNOS in the ischemic cortex treated with MIP or CP at 7 dpi. (I) Western blotting and real-time RT-PCR of Arg-1 in the ischemic cortex treated with MIP or CP at 7 dpi. (J, K) Real-time RT-PCR of TNFα, IL-18, IL-4, and IL-10 in ischemic cortex treated with MIP or CP at 7 dpi. Arrowheads in C indicate double-positive cells. $N = 3$ mice in each group or 3 batches of cells for each experiment. $^{*}P < 0.05$. $^{**}P < 0.01$.

programmed necrosis of neurons postischemia (Vaseva et al. 2012). Inflammation may cause the necroptosis of astrocytes, as we have reported that following spinal cord injury, M1 microglia induces chronic necroptosis of astrocytes (Fan et al. 2016). The difference of present study and our previous one may lie in the type of injury and the difference in cellular composition between the cortex and the spinal cord. The reduction in lesion size in RIPK3$^{-/-}$ and MLKL$^{-/-}$ mice strongly indicated that RIPK3/MLKL-mediated necroptosis is an important pathological change in the ischemic cortex.

Inflammation in the ischemic cortex is developed primarily by activated microglia/macrophages, recruited mononuclear cells and T lymph cells (Anrather and Iadecola 2016). Among these cells, microglia/macrophages act as the first line of immune response. Active microglia and macrophages adopt almost the same phenotype in the ischemic cortex, playing either damage-clearing/neurotoxic or reparative/neuroprotective roles depending on their M1/M2 polarization. Necroptosis is characterized by the rupture of the cell membrane, which releases large amounts of DAMP factors, for example, members of the IL-1 family (Oberst 2016; Vince and Silke 2016). In addition, it was recently observed that MLKL not only forms channels on the cell membrane but also triggers the formation of the nucleotide-binding oligomerization domain (NOD)-like receptor protein 3 (NLRP3) inflammasome and regulates extracellular vesicle generation (Conos et al. 2017; Huang et al. 2017; Yoon et al. 2017). Our *in vivo* experiments depleting RIPK3, MLKL and Caspase-3 suggested that RIPK3/MLKL signaling may play an important role in modulating M1/M2-polarization of microglia/macrophages in ischemic cortex. And, our *in vitro* data that necroptotic neurons favor M1 polarization of microglia/macrophages support a proinflammatory role of neuronal necroptosis. Although we did not observe significant changes in microglia/macrophage polarization by OGD-treated astrocytes, the possible effects of other cells is not excluded, as necroptotic microglia/macrophages by themselves modulate inflammation (Huang et al. 2018). There is emerging evidence (Rickard et al. 2014) regarding the upregulation of mRNA levels of inflammatory factors in OGD-treated neurons, indicating an active role of necroptosis in regulating inflammation. Although RIPK3 modulates inflammation independent of necroptosis (Moriwaki and Chan 2013, 2014), no significant changes in basal iNOS and Arg-1 expression in the uninjured cortices and blood macrophages of RIPK3$^{-/-}$ and MLKL$^{-/-}$ mice indicated a role of necroptosis in the polarization of microglia/macrophages upon injury. The different profiles of cytokine expression between OGD-treated WT and RIPK3$^{-/-}$ or MLKL$^{-/-}$ neurons are interesting. It is possible that the NF-κb signaling in WT, RIPK3- or MLKL-deficient neurons may be differently regulated under OGD stress, thereby leading to different cytokine expression, a hypothesis that remains to be further explored. The reduction of secondary neuronal apoptosis and upregulation of BDNF by microglial/macrophages indicated a neuroprotective effect of RIPK3- or MLKL-ablation. Nevertheless, our data suggested that inhibiting necroptosis may exert more beneficial effects than those exerted by reducing neuronal necrosis.

Polarization of microglia/macrophages is regulated by multiple extracellular and intracellular factors. Previous studies have demonstrated that IL-33 and IL-4 play a role in regulating polarization of microglia/macrophages in the ischemic cortex (Zhao et al. 2015; Liu et al. 2016; Yang, Liu, et al. 2017). Our data provided new mechanistic insights into the cellular origin of post-ischemic IL-4. In the ischemic cortex, microglia/macrophages are stimulated by numerous cytokines simultaneously, and their phenotypes are determined by the balance of all stimulating factors favoring or against polarization. Considering the facts that the expression of multiple TLRs was changed after ischemia, and that Myd88 is a common adaptor of all TLRs for transducing signaling downstream (Deguine and Barton 2014), we focused on the role of Myd88 in this necroptosis-induced polarization. Changes in Myd88 levels correlate well with the expression of M1/M2 markers in both WT, RIPK3$^{-/-}$ and MLKL$^{-/-}$ mice, suggesting the possible involvement of Myd88 in this process. Interfering with the function of Myd88 phenocopied the effects of RIPK3- and MLKL-knockout, indicating an essential role of Myd88 in the polarization of microglia/macrophages. It is possible that different levels of Myd88 signaling differently regulate transcriptional factors, such as Stat1/6 and interferon regulatory factor 7/8 (Saleiro and Platanias 2015), thereby determining the fate of microglia/macrophages. Alternatively, there may be a threshold of Myd88 for switching M1/M2, a hypothesis that remains to be further investigated. The neuroprotective effects of the Myd88 inhibitory peptide as demonstrated by the reduction of secondary neuronal apoptosis and enhancement of BDNF expression, although not very specific, suggested the future possibility of its therapeutic application in stroke.

Supplementary Material

Supplementary material is available at *Cerebral Cortex* online.

Funding

National Natural Science Foundation of China in the form of grants to Dr Shengxi Wu (Grant no. 81730035) and to Dr Yazhou Wang (Grant no. 81571224), the Innovation Teams in Priority Areas Accredited by the Ministry of Science and Technology (Grant no. 2014RA4029) and the grant by Project Supported by Natural Science Basic Research Plan in Shaanxi Province of China to Dr Jiping Yang (Program No. 2017JM8061).

Notes

The authors thank Prof Jiahuai Han (Xiamen University) for providing the MLKL$^{-/-}$ mice and Dr Dixit (Genentech) for providing the RIPK3$^{-/-}$ mice. The authors appreciate Prof. Hongyan Qin, Prof Yingying Liu and Dr Fangfang Liu for technical assistance. *Conflict of Interest*: The authors claim no conflicts of interests.

References

Amantea D, Bagetta G. 2016. Drug repurposing for immune modulation in acute ischemic stroke. Curr Opin Pharmacol. 26:124–130.

An C, Shi Y, Li P, Hu X, Gan Y, Stetler RA, Leak RK, Gao Y, Sun BL, Zheng P, et al. 2014. Molecular dialogs between the ischemic brain and the peripheral immune system: dualistic roles in injury and repair. Prog Neurobiol. 115:6–24.

Anrather J, Iadecola C. 2016. Inflammation and stroke: an overview. Neurotherapeutics. 13:661–670.

Baskin YK, Dietrich WD, Green EJ. 2003. Two effective behavioral tasks for evaluating sensorimotor dysfunction following traumatic brain injury in mice. J Neurosci Methods. 129:87–93.

Brea D, Blanco M, Ramos-Cabrer P, Moldes O, Arias S, Perez-Mato M, Leira R, Sobrino T, Castillo J. 2011. Toll-like receptors 2 and 4 in ischemic stroke: outcome and therapeutic values. J Cereb Blood Flow Metab. 31:1424–1431.

Chan FK, Luz NF, Moriwaki K. 2015. Programmed necrosis in the cross talk of cell death and inflammation. Annu Rev Immunol. 33:79–106.

Christofferson DE, Yuan J. 2010. Necroptosis as an alternative form of programmed cell death. Curr Opin Cell Biol. 22:263–268.

Conos SA, Chen KW, De Nardo D, Hara H, Whitehead L, Nunez G, Masters SL, Murphy JM, Schroder K, Vaux DL, et al. 2017. Active MLKL triggers the NLRP3 inflammasome in a cell-intrinsic manner. Proc Natl Acad Sci USA. 114:E961–E969.

Degterev A, Huang Z, Boyce M, Li Y, Jagtap P, Mizushima N, Cuny GD, Mitchison TJ, Moskowitz MA, Yuan J. 2005. Chemical inhibitor of nonapoptotic cell death with therapeutic potential for ischemic brain injury. Nat Chem Biol. 1:112–119.

Deguine J, Barton GM. 2014. MyD88: a central player in innate immune signaling. F1000prime Rep. 6:97.

Fan H, Tang HB, Kang J, Shan L, Song H, Zhu K, Wang J, Ju G, Wang YZ. 2015. Involvement of endoplasmic reticulum stress in the necroptosis of microglia/macrophages after spinal cord injury. Neuroscience. 311:362–373.

Fan H, Zhang K, Shan L, Kuang F, Chen K, Zhu K, Ma H, Ju G, Wang YZ. 2016. Reactive astrocytes undergo M1 microglia/macrohpages-induced necroptosis in spinal cord injury. Mol Neurodegener. 11:14.

Gingras M, Gagnon V, Minotti S, Durham HD, Berthod F. 2007. Optimized protocols for isolation of primary motor neurons, astrocytes and microglia from embryonic mouse spinal cord. J Neurosci Methods. 163:111–118.

Grootjans S, Vanden Berghe T, Vandenabeele P. 2017. Initiation and execution mechanisms of necroptosis: an overview. Cell Death Differ. 24:1184–1195.

Hamby ME, Uliasz TF, Hewett SJ, Hewett JA. 2006. Characterization of an improved procedure for the removal of microglia from confluent monolayers of primary astrocytes. J Neurosci Methods. 150:128–137.

Hu X, Leak RK, Shi Y, Suenaga J, Gao Y, Zheng P, Chen J. 2015. Microglial and macrophage polarization-new prospects for brain repair. Nat Rev Neurol. 11:56–64.

Huang D, Zheng X, Wang ZA, Chen X, He WT, Zhang Y, Xu JG, Zhao H, Shi W, Wang X, et al. 2017. The MLKL channel in necroptosis is an octamer formed by tetramers in a dyadic process. Mol Cell Biol. 37:pii: e00497-16.

Huang Z, Zhou T, Sun X, Zheng Y, Cheng B, Li M, Liu X, He C. 2018. Necroptosis in microglia contributes to neuroinflammation and retinal degeneration through TLR4 activation. Cell Death Differ. 25:180–189.

Lan X, Han X, Li Q, Yang QW, Wang J. 2017. Modulators of microglial activation and polarization after intracerebral haemorrhage. Nat Rev Neurol. 13:420–433.

Lee JK, Park MS, Kim YS, Moon KS, Joo SP, Kim TS, Kim JH, Kim SH. 2007. Photochemically induced cerebral ischemia in a mouse model. Surg Neurol. 67:620–625; discussion 625.

Liu X, Liu J, Zhao S, Zhang H, Cai W, Cai M, Ji X, Leak RK, Gao Y, Chen J, et al. 2016. Interleukin-4 is essential for microglia/macrophage M2 polarization and long-term recovery after cerebral ischemia. Stroke. 47:498–504.

Ma Y, Wang J, Wang Y, Yang GY. 2017. The biphasic function of microglia in ischemic stroke. Prog Neurobiol. 157:247–272.

Moriwaki K, Chan FK. 2013. RIP3: a molecular switch for necrosis and inflammation. Genes Dev. 27:1640–1649.

Moriwaki K, Chan FK. 2014. Necrosis-dependent and independent signaling of the RIP kinases in inflammation. Cytokine Growth Factor Rev. 25:167–174.

Murakami Y, Matsumoto H, Roh M, Giani A, Kataoka K, Morizane Y, Kayama M, Thanos A, Nakatake S, Notomi S, et al. 2014. Programmed necrosis, not apoptosis, is a key mediator of cell loss and DAMP-mediated inflammation in dsRNA-induced retinal degeneration. Cell Death Differ. 21:270–277.

Narayanan KB, Park HH. 2015. Toll/interleukin-1 receptor (TIR) domain-mediated cellular signaling pathways. Apoptosis. 20:196–209.

Ni Y, Gu WW, Liu ZH, Zhu YM, Rong JG, Kent TA, Li M, Qiao SG, An JZ, Zhang HL. 2017. RIP1K contributes to neuronal and astrocytic cell death in ischemic stroke via activating autophagic-lysosomal pathway. Neuroscience. 371:60–74.

Oberst A. 2016. Death in the fast lane: what's next for necroptosis? FEBS J. 283:2616–2625.

Piccinini AM, Midwood KS. 2010. DAMPening inflammation by modulating TLR signalling. Mediators Inflam. 2010:21.

Rickard JA, O'Donnell JA, Evans JM, Lalaoui N, Poh AR, Rogers T, Vince JE, Lawlor KE, Ninnis RL, Anderton H, et al. 2014. RIPK1 regulates RIPK3-MLKL-driven systemic inflammation and emergency hematopoiesis. Cell. 157:1175–1188.

Saleiro D, Platanias LC. 2015. Intersection of mTOR and STAT signaling in immunity. Trends Immunol. 36:21–29.

Scaffidi P, Misteli T, Bianchi ME. 2002. Release of chromatin protein HMGB1 by necrotic cells triggers inflammation. Nature. 418:191–195.

Stoll G, Jander S, Schroeter M. 1998. Inflammation and glial responses in ischemic brain lesions. Prog Neurobiol. 56:149–171.

Sun L, Wang X. 2014. A new kind of cell suicide: mechanisms and functions of programmed necrosis. Trends Biochem Sci. 39: 587–593.

Sweetnam D, Holmes A, Tennant KA, Zamani A, Walle M, Jones P, Wong C, Brown CE. 2012. Diabetes impairs cortical plasticity and functional recovery following ischemic stroke. J Neurosci. 32:5132–5143.

Vaseva AV, Marchenko ND, Ji K, Tsirka SE, Holzmann S, Moll UM. 2012. p53 opens the mitochondrial permeability transition pore to trigger necrosis. Cell. 149:1536–1548.

Vidale S, Consoli A, Arnaboldi M, Consoli D. 2017. Postischemic inflammation in acute stroke. J Clin Neurol. 13:1–9.

Vince JE, Silke J. 2016. The intersection of cell death and inflammasome activation. Cell Mol Life Sci. 73:2349–2367.

Wallach D, Kang TB, Dillon CP, Green DR. 2016. Programmed necrosis in inflammation: toward identification of the effector molecules. Science. 352:aaf2154.

Wang YZ, Liu YY, Liu JP, You SW, Ju G. 2006. Nogo-66 receptor at the gap junctions between pituicytes of the rat. NeuroReport. 17:605–609.

Weinlich R, Oberst A, Beere HM, Green DR. 2017. Necroptosis in development, inflammation and disease. Nat Rev Mol Cell Biol. 18:127–136.

Xiong XY, Liu L, Yang QW. 2016. Functions and mechanisms of microglia/macrophages in neuroinflammation and neurogenesis after stroke. Prog Neurobiol. 142:23–44.

Yang R, Hu K, Chen J, Zhu S, Li L, Lu H, Li P, Dong R. 2017. Necrostatin-1 protects hippocampal neurons against ischemia/reperfusion injury via the RIP3/DAXX signaling pathway in rats. Neurosci Lett. 651:207–215.

Yang Y, Liu H, Zhang H, Ye Q, Wang J, Yang B, Mao L, Zhu W, Leak RK, Xiao B, et al. 2017. ST2/IL-33-dependent microglial response limits acute ischemic brain injury. J Neurosci. 37: 4692–4704.

Yang M, Lv Y, Tian X, Lou J, An R, Zhang Q, Li M, Xu L, Dong Z. 2017. Neuroprotective effect of beta-caryophyllene on cerebral ischemia-reperfusion injury via regulation of necroptotic neuronal death and inflammation: in vivo and in vitro. Front Neurosci. 11:583.

Yang XS, Yi TL, Zhang S, Xu ZW, Yu ZQ, Sun HT, Yang C, Tu Y, Cheng SX. 2017. Hypoxia-inducible factor-1 alpha is involved in RIP-induced necroptosis caused by in vitro and in vivo ischemic brain injury. Sci Rep. 7:5818.

Yang J, Zhang X, Wu Y, Zhao B, Liu X, Pan Y, Liu Y, Ding Y, Qiu M, Wang YZ, et al. 2016. Wnt/beta-catenin signaling mediates the seizure-facilitating effect of postischemic reactive astrocytes after pentylenetetrazole-kindling. Glia. 64:1083–1091.

Yenari MA, Kauppinen TM, Swanson RA. 2010. Microglial activation in stroke: therapeutic targets. Neurotherapeutics. 7:378–391.

Yoon S, Kovalenko A, Bogdanov K, Wallach D. 2017. MLKL, the protein that mediates necroptosis, also regulates endosomal trafficking and extracellular vesicle generation. Immunity. 47:51–65 e57.

Zhao X, Wang H, Sun G, Zhang J, Edwards NJ, Aronowski J. 2015. Neuronal interleukin-4 as a modulator of microglial pathways and ischemic brain damage. J Neurosci. 35:11281–11291.